Crustal Deformation Measurements Using Repeat-pass JERS 1 SAR Interferometry Near the Izu Peninsula, Japan

Satoshi Fujiwara[1], Paul A Rosen

Jet Propulsion laboratory, California Institute of Technology, Pasadena CA USA

Mikio Tobita, Makoto Murakami

Geographical Survey Institute, Tsukuba Japan

#JB97-0127

Please address editorial correspondence:

Satoshi Fujiwara

Geodetic Department

Geographical Survey institute

Kitasato-1, Tsukuba, Ibaraki 305 JAPAN

Tel: +81-298-64-4774

Fax: +81-298-64-1802

E-mail: fujiwara@gsi-mc.go.jp

[1] Now at Geographical Survey institute, Tsukuba Japan

Abstract,

We have examined the precision of interferometric SAR measurements of surface deformation of the Earth using 24-cm wavelength data acquired by the Japanese Earth Resources Satellite 1 (JERS 1) spacecraft, over the Izu peninsula, Japan. Radar images acquired from 1993 to 1994 were made into eleven independent interferograms. Apparent water vapor signatures with equivalent path delay up to 16 cm preclude reliable estimates of small deformation from only one interferogram. Averaging of interferograms improves the measurement, such that residuals between precise leveling data and corresponding radar observations are less than 1 cm RMS. There is a clear correlation between cloud cover extent on a given day and the spectral power of the water vapor signature in an interferogram formed from the corresponding day's SAR image. Also, several water vapor features associated with local topography are consistent with accumulation of moisture on the windward side of an on-shore flow. Analysis shows that decorrelation in mixed conifer and deciduous forest is a weak function of the time between observations, imposing a roughly constant level of additional decorrelation relative to scatter-stable urban areas. Furthermore, in high relief areas correlation is high when the baseline is tens of meters, but drops rapidly with increasing baseline length. With strict control of the interferometric baseline length, adequate correlation in interferograms over very long time periods is possible even in forested, high relief regions. Observed inflation over Ito city is consistent with a localized magma source at depth, suggesting a different mechanism from the previous episode in 1989.

introduction

Crustal deformation study using SAR interferometry

Crustal deformation measurements relating to earthquakes and volcanic activity are

essential to understand processes occurring below the surface. Geodetic observation at triangulation stations and bench marks, strainmeters and extensionmeters, etc. have been the conventional observational tools for crustal deformation. Now with continuous Global Positioning System (GPS) observation, it is possible to measure the temporal variability of crustal deformation in detail, but only at a spatially discrete set of locations. By distributing the GPS observation points densely, it would be possible to obtain the spatial distribution in detail as well, but a limit to this exists with respect to cost and labor.

SAR interferometry from space has become an important tool for measuring the dense spatial distribution of surface deformation and for topography, Many recent studies in radar interferometry have used ERS 1 C-band SAR [*Massonnet et al.,* 1993; *Zebker et al.,* 1994a; *Zebker et al.,* 1994b; *Massonnet et al., 1995; Peltzer and Rosen,* 1995]. The SIR-C/X-SAR mission showed that L-band (24 cm wavelength) SAR is far superior to C-band (5.6 cm wavelength) SAR in vegetated areas [*Rosen et al.,* 1996]. The L-band radar signal penetrates the vegetation more easily and is more robust than C-band in terms of decorrelation. In Japan, as almost all areas except cities are well vegetated, it is difficult to obtain good correlation using C-band SAR, so L-band or some other long wavelength is essential for deformation measurements by interferometric SAR. JERS 1 is the only L-band SAR satellite currently on orbit, and is now operating beyond its designed life span. It has some limitations, such as low signal-to-noise ratio and poor orbit knowledge, compared with the ERS 1,2 and SIR-C, but nonetheless has provided deformation measurements where these sensors could not. For example, *Murakami et al. [1995], Murakami et al.* [1996a), *Murakami et al. [1996b]* and *Fielding et al. [1996]* have measured coseismic deformations of several earthquakes using JERS 1 with fairly challenging surface conditions.

In this paper, we take a systematic approach to investigate the precision and accuracy of JERS 1 repeat-pass interferometric measurements. There are four possible error sources that limit the accuracy of the interferograms: First, decorrelation clue to thermal noise, volumetric scatter and temporal changes of surface targets degrades the quality of the interferograms [*Zebker and Villasenor,* 1992]. Second, differential atmospheric delay biases the phase measurement. The effect of water vapor in the atmosphere is well known from microwave space geodetic techniques, such as Very Long Baseline Interferometry (VLBI) [Herring, 1986] and GPS [*Dixon and Wolf*, 1990]. *Goldstein* [1995], *Rosen et al. [1996],* and *Zebker et al.* [1997] described the phase delay in the interferograms derived from SIR-C data, but were limited to only a few observations of disparate sites. The third source is baseline estimation error, which causes a phase distortion in the interferogram [*Zebker et al.,* 1994a,b; *Rosen et al., 1996].* Finally, digital elevation model (DEM) errors for the so-called "two pass" method *[Rosen et al.,* 1996; *Murakami et al.,* 1996a] and tie points errors generate phase errors in interferograms.

We selected the lzu peninsula in Japan and the area extending north of Mount Fuji as our study area. The area is a good site to explore the potentials and limitations of JERS 1 SAR interferometry. It is a 'wet' region, with rainfall of more than 2000 mm/year. Summer is the rainy season while winter is rather dry. The region comprises extended urban centers, mountainous and vegetated regions, in various combinations suitable for studies of correlation, deformation, and topographic mapping.

Interferometric SAR observations of the lzu peninsula are important because they measure the spatial distribution of the crustal deformation in detail, extending other geodetic and

geophysical observations to further constrain source mechanisms. Leveling data exist that are roughly coincident with the radar observations of this area. The analysis here combines leveling and radar observations in this way. The comparison with ground truth also provides a means of assessing the local accuracy of the radar measurements.

Furthermore, because the deformation signal is weak, and the noise known to be fairly high, we discuss methods to reduce the phase errors of interferograms. Since several cm of crustal deformation are usually found in the region of interest in Japan (see the next section), our goal is to obtain 1 cm accuracy of surface deformation from L-band SAR interferometry with precise leveling as a reference. Fine spatial resolution is less important in most geophysical applications. This is fortunate because large decorrelation in mountainous areas obliges us to smooth the images, giving lower spatial resolution.

Geologic Background

The Izu peninsula in central Japan, shown in Figs.1 and 2, lies at the. boundary of three tectonic plates: the Philippine Sea plate, North American plate and Eurasian plate. After the 1974 Izu-Hanto-Oki earthquake (M=6.9, to the south of Fig.2) this region became seismically active and is now one of the most tectonically active regions in Japan. Over 20 earthquake swarms have occurred around Ito city (Fig. 2) since the 1978 Izu-Oshima-Kinkai earthquake (M=7.0, Fig.2) [*Earthquake Prediction information Division, 1994].* A tide station in Ito city uplifted more than 30 cm in this interval *[Geographical Survey Institute,* 1994a, 1994b and 1995]. This activity is related to volcanic processes [*Okada and Yamamoto, 1991]. Tada and Hashimoto [1991]* concluded from repeated precise geodetic surveys that the northeastern Izu Peninsula is under NE-SW tension and that monogenetic volcanoes are born in the NW-SE-trending crack under the tension stress field.

From repeated precise leveling and continuous GPS observations, the surface was found to be uplifted up to 5 cm around Ito city in autumn 1993 (Figs. 8b and 9) *[Geographical Survey Institute, 1994a,* 1994b and1995]. *Okada and Yamamoto [1991]* concluded that the heavy swarm earthquakes and crustal deformations in 1989 were caused by a dyke intrusion, that is the intersection of a shear fault with the tensile fault, causing magma to flow up into sedimentary layers north of Ito city. However, in autumn 1993 the seismic activity was not high and the epicenters were rather widely distributed (Fig. 2), so the crustal uplift in Fig. 8b cannot be explained by the dyke intrusion model. The deformation in autumn 1993 was likely related to volcanic activity, but the mechanism has not been clear.

Data and Method

JERS 1 SAR Data

The JERS 1 SAR looks off-nadir to the right at approximately 35°, and typically observes during descending daytime passes from a 44 day repeat orbit at about 570 km altitude. Table 1 is a time chart of the JERS 1 satellite images used, acquired over a period from February 25, 1993 to February 12, 1994. All images used in this study are from descending data takes, therefore, are taken from the ESE direction. *Shimada et al. [1993], Murakami et al.* [1996a] and *Rossi et al. [1996]* provide additional details.

Full scenes of JERS 1 SAR raw signal data covering an area of approximately 70 km by 70 km were provided by the National Space Development Agency of Japan (NASDA). We combined two time sequential raw data sets to generate a larger 70 km (range, cross-track direction) by 140 km (azimuth, along-track direction) raw data product. SAR and interferometric processing were carried out with phase preserving processing software

developed at JPL in a collaborative effort specifically for this work. It was designed to emulate and improve upon existing JPL software [*Zebker et al.*, 1994a: *Rosen et al.*, 1996] in both the user interface and differential processing algorithms.

Interferograms

The pixel spacing in the interferograms used in this study is about 55m (4 looks) in ground range and 75m (16 looks) in azimuth. Plate 1 shows an example of a flattened interferogram for which the phase has been corrected for the sphericity of the earth's surface [*Rosen et al.*, 1996]. Almost all the fringes in this plate are due to topography; the concentric fringes in the middle left correspond to Mt. Fuji (3776 m), the highest mountain in Japan. The fringe quality on flat areas is rather good but areas with complicated topography are noticeably worse.

DEM and simulated image

There are two ways to eliminate topographic features from an interferogram. One is synthesizing an interferogram using a DEM [*Massonnet et al., 1993*] and the other is using an independent interferogram with small surface deformation or noise as a reference [*Zebker et al.*, 1994b]. Though we have seven raw SAR images, the interferometric pairs with longer baselines necessary to construct a good DEM have insufficient correlation. The main difficult y of making a DEM is in phase unwrapping [*Goldstein et al.*, 1988] because of severe decorrelation in mountain areas as seen in Plate 1. Further discussion on decorrelation will be presented later.

We use the Geographical Survey Institute of Japan 50 m grid DEM to create interferometric simulation images and estimate baselines. Each point of the DEM has a 0.1 m height

precision at intervals of 1.5 sec of arc in the longitude direction and 2.25 sec in the latitude direction (the mesh spacing is about .50 *m).* The theoretical vertical error is at most 7 m and the vertical RMS error is less than 5 m [*Shimoyama et al.,* 1995]. The errors in the interferometric images due to DEM errors increase in proportion to baseline length. The largest baseline component perpendicular to the look direction in this study is about 1250 m and the error in the phase change due to the DEM error for this baseline is 1 rad (1.9 cm in range change), which is small compared to other error sources.

A simulated interferometric phase is subtracted from the interferogram to remove the topographic fringes. The simulated interferogram is shown in Plate 2a. The simulation method is similar to that presented by *Rosen et al.* [1996].

Baseline estimation using DEM

A baseline value accurate at the cm level is necessary to calculate the simulation image and to remove the spherical-earth surface phase ("flatten phase"). However, the ephemeris data of JERS 1 do not allow such accuracy. The baseline can be estimated using the unwrapped phase, with a DEM providing a large number of ground control points [Rosen et *al.,* 1996]. Since phase unwrapping errors become larger when the interferometric fringe rate is higher, we encounter difficulty in unwrapping the flattened phase in steep mountain areas. In addition, excessive noise due to decor-relation contributes to the difficulty. Plate 1 shows a flattened interferogram where the phase distribution in mountainous areas is too noisy to unwrap the phase. To avoid unwrapping the phase, we first calculate rough baseline values from the offset field of two SAR images and calculate an intermediate interferometric simulation image. After subtraction of the simulated topographic fringe image from the interferogram, the residual phase fringe rate becomes much smoother and

we can usually unwrap the phase. With low-pass filtered 16 look (range; a pixel resolution of 220 m) by 64 look (azimuth; a pixel resolution of 300 m) images we can unwrap the phase even in decorrelated mountain areas. We then restore the simulated topography (the same one subtracted before the phase unwrapping) to the unwrapped phase to calculate the precise baseline. The interplay of decorrelation, phase anomalies and baseline length in relation to baseline estimation and DEM production is discussed in the appendices.

Results

Interferograms

The eleven differential interferograms in Plates 2b - 21 are geocoded and drawn in a UTM projection with the lower left comer at (34.52° N, 138.40° E) and the upper right comer at (35.90° N, 139.40° E). In this paper, the notation [2/25/93-4/10/93] denotes an image pair calculated using the image data acquired on February 25, 1993 and April 10, 1993. The pixel spacing in the geocoded images is about 130 m. A low-pass filter was applied to each image because the interferograms are noticeably noisy from decorrelation in mountainous areas. Therefore, the pixel resolution depends on the decorrelation and it is about 200 m in this region. The geometric and topographic phase changes are removed from the interferograms, so the remaining phase patterns in Plates 2b –21 can be ascribed to range changes between the antenna and the surface target, or to atmospheric delays. Comparison of L and C-band data from SIR-C, showed no frequency dispersion in the observed interferograms [*Goldstein*, 1995; *Rosen et al.,* 1*996],* indicating the effects of the ionosphere in these studies were negligible. However, JERS 1 orbits at a higher altitude with an appreciable y longer ionosphere path length than SIR-C (570 km *vs* 215 km), so the ionosphere (F layer) is likely to play a larger role in affecting the phase of JERS 1

interferometry. As the JERS 1 takes SAR data almost the same time of day. the effect of daily variation of the ionosphere is small. However, there is room for further investigation of ionospheric effects such as seasonal variations.

At first glance, the amplitude of the changes in Plates 2b – 21 images is noticeably large and the changes are randomly distributed, however, it often turns out that a particular change can be associated with a particular image. For example, [7/7/93-8/20/93] (Plate 2i), [7/7/93 -10/3/93] (Plate 2j) and [7/7/93 -11/16/93] (Plate 2k) show an increase in the phase in the central region and a decrease near the southern tip of the Izu peninsula but other interferograms including these periods, such as [4/10/93 -8/20/93](Plate 2e) and [4/10/93 - 11/16/93] (Plate 2g), do not show these patterns. Therefore, most of these changes must belong to only the image taken on 7/7/93. In the same way, [4/)0/93-10/3/93] (Plate 2f) and [7/7/93-10/3/93] (Plate 2j) show quite similar changes, and we find that the greater part of their changes belongs to the image taken on 10/3/93. Shorter wavelength changes exhibit similar behavior. Figure 3 shows phase cross sections for two interferograms, along line C-D (Fig. 2). These phase delay values are those shown in Plate 2 after removal of a number of geometric effects. The changes are nearly sinusoidal with wavelength of about 5 km. Since those of [7/7/93-8/20/93] (Plate 2i) and [8/20/93-11/16/93] (Plate 21) have nearly the opposite sign, the phase variations belong to the image taken on 8/20/93. The association of changes with a specific image suggests the influence of a process that varies rapidly in time, e.g., atmospheric delay, and we make that assumption in the remainder of this paper.

Figure 4 shows two phase cross sections along line A-B (Fig. 2). The spatial scale of the phase patterns varies from a few km to more than 100 km and likely extends beyond the

boundaries of the image. The changes in [7/7/93-10/3/93] (Plate 2j) are the largest in the eleven interferograms. The peak to peak amplitude along the phase cross section A-B corresponds to about 16 cm in range and the longest wavelength is more than 100 km. These changes are too large to be accounted for by surface deformation, since significant surface deformations have not been found at tidal stations nor other geodetic stations in and around the Izu peninsula during these time intervals [*Geographical Survey Institute*, 1994a and 1994b]. Furthermore, the patterns of change in Figs. 3 and 4 would require unusual surface deformation mechanisms. For example, if the changes in Fig. 3 are due to crustal deformation, they would require deformations of the same amplitudes but the opposite directions before and after 8/20/93, respectively. Though real surface deformations around Ito city are actually present in [2/25/93-2/12/94] (Plate 2c), [4/10/93-11/16/93] (Plate 2g), [4/10/93-2/12/94] (Plate 2h) and [7/7/93-11/16/93] (Plate 2k), they are difficult to distinguish from propagation effects with only one interferogram.

Distribution of phase delay and weather

The SIR-C interferograms acquired over the Mojave Desert in California [*Goldstein*, 1995], and over Hawaii *[Rosen et al, 1996; Zebker et al., 1997]* showed that the residual phase delay distribution was not related to surface topography. In contrast, the JERS 1 L-band radar interferograms acquired over Mt. Fuji and the Izu peninsula show that the residual phase delay of some areas is related to surface features such as mountain ranges. The distribution of water vapor in this region may show some relation to local topographic features because of the wetness of this region. We show four examples of residual delay related to the topography and the weather. First, consider the residual delay changes at the top of Mt. Fuji in the interferograms [7/7/93-8/20/93] (Plate 2i), [7/7/93-10/3/93] (Plate 2j) and [7/7/93-1 1/1 6/93] (Plate 2k). These changes are associate with the image taken on

7/7/93. Mt. Fuji is the highest mountain in these scenes and the residual phase delay over the summit was smaller than that over the hillsides on 7/7/93. Since it was rainy on the day of the image, there was probably heavy water vapor at a lower altitude than the summit at the time the image was acquired. Therefore, the difference of the radar line-of-sight range at the summit and the hillsides made the difference of the residual phase delay of water vapor. Moreover, there is a possibility that the water vapor at the summit was changed to clouds by rising wind around the high mountain. As a second example, the north-eastern and the south-western slopes of mountain ridges in the Izu peninsula show the opposite sense of delay in the images [7/7/93-8/20/93] (Plate 2i) and [8/20/93-11/16/93] (Plate 21). Lines E and F in Fig. 2 are located along mountain ridges which coincide with transitions in the phase delay. For example, in the interferogram [8/20/93-11/1 6/93] (Plate 21) the northeastern slopes of the ridges are green and the others are yellow. Figure 5 shows the phase cross section of the image pair [8/20/93-11/16/93] (Plate 21) and the cross section of topography, along line G-H (Fig. 2). These changes probably belong to the image taken on 8/20/93 when the wind was blowing from the southwest and it rained, but the precipitation was smaller than 1 mm at Irozaki and Mishima (near Numazu) [*Japan Meteorological Agency, 1993]*. Therefore, the rising wet air caused rain to fall on the southwestern slope of the mountains and the air likely was drier over the northeastern slope after passing the ridges. Third, the nearly sinusoidal changes in Fig. 3 also probably belong to the image taken on 8/20/93. The changes were likely atmospheric waves typically found downwind of mountains. Finally, the delay is sometimes large at the southern tip of the Izu peninsula, particularly in the interferograms including images taken on 4/10/93 and 7/7/93; on the contrary it is small in the image taken on 10/3/93. On the day 4/10/93, the weather was clear except for the southern Izu peninsula where it was mostly cloudy (see Table 1) [*Japan Meteorological Agency,* 1993). The water vapor distribution may tend to

have a relation to topography where there are geographically singular features such as the tip of a peninsula.

Figure 6a shows spatial power spectra of the residual phase delay along cross section A-B in Fig. 2. Each added line is obtained by fitting a power-law function to the power spectrum by the least square method. The broken lines follow the 8/3 slope expected from radar observation of turbulence [*Goldstein*, 1995]. Though the power spectrum roughly fits the 8/3 slope, the absolute power level varies by up to a factor of 100 between interferograms.

We assume that most of the anomalous phase delay is due to atmospheric processes, most likely tropospheric delay, because of the region's high rainfall. Table 1 shows the daily mean cloud cover at Kofu (in the northern part) and Irozaki (in the southern part) plotted in Fig. 2 *[Japan Meteorological Agency, 1993* and 1994]. Figure 6b shows that the power of the phase delay undulation in the interferograms becomes larger as the interferogram includes more clouds. Though an interferogram consists of two images, the image with more clouds probably has the larger influence on the observed phase delay of the interferogram. Therefore, not only does the total delay becomes larger but the phase delay spatial undulation also becomes larger on cloudier days, suggesting that cloud cover can be used as an indicator of water vapor variability. Since a phase delay in an interferogram is not the absolute delay but the relative delay between images, we cannot estimate the total component of the phase delay without further assumptions or additional information.

These phase delays are probably related to the atmospheric water vapor, however, we cannot identify phase delays specifically related to the ionosphere. Though the undulation

of the ionospheric delay is probably smaller than that of the atmospheric delay, there is room for further investigation.

The JERS 1 interferograms in Northridge [*Murakami et al.*, 1996a], Kobe [*Murakami et al.*, 1995] and Northern Sakhalin [*Murakami et al.*, 1996b; *Fielding et al.*, 1996] may contain atmospheric phase delays but these are smaller than those in this study because of less water vapor and flatter topography. However, we have not found a good quantitative measure of the 'wetness' and its coupling to topography as it affects interferograms in L-band SAR interferometry.

Decorrelation

The correlation coefficient at each pixel is one of the fundamental measures of the quality of an interferogram. It is given by

$$\gamma = \frac{|\langle c_1 c_2^* \rangle|}{\sqrt{\langle c_1 c_1^* \rangle \langle c_2 c_2^* \rangle}} \qquad (1)$$

where c_1 and c_2 are complex image values of the images that form the interferogram, c* denotes the complex conjugation of c, and the brackets () stand for the ensemble mean. We calculate the correlation coefficient y using the phase from which the topography has been removed, so there are essentially no high-rate fringes to bias the correlation estimator, which is optimal when the interferometric phase is constant. *Wegmüller and Werner [1995]* showed empirically that the number of pixels used to compute the ensemble mean (average window size) biases the correlation coefficient in low interferometric correlation areas and a larger window size is required for those areas (see also [*Zebker et al.*, 1996]). For our

correlation calculation, we use images with 4 looks taken in the range direction and 16 looks in the azimuth direction. From these images, the correlation ensemble mean is computed using an additional 5 by 5 averaging window.

Zebker and Villasenor [1992] explained that there are three major causes of decorrelation in repeat-pass interferograms: thermal noise, spatial baseline decorrelation and temporal decorrelation.

Plate 3 shows correlation maps; [2/25/93-4/10/93] (Plates 2b and 3c) has the best correlation and [4/10/93-8/20/93] (Plates 2e and 3a) has the worst correlation (the largest decorrelation) in the eleven correlation maps. These correlation coefficients shown in Plate 3 and the fringe visibility in Plate 2b – 21 have a close relationship, namely regions with high correlation corresponds to regions with high fringe visibility. Plate 3 clearly shows urban cities retain rather high correlation values even for [4/1 0/93-8/20/93] (Plates 2e and 3a).

In order to understand the characteristics of the decorrelation, we calculated the correlation in high relief areas, a forest area and an urban area individually. These areas are shown in Fig. 2. In general the mountains in central Japan are well covered with trees, such as Japanese oaks, beeches, cypresses and cedars. The high relief areas have very steep slopes and complicated topography. The forest study area is situated on the slopes leading to Mt. Fuji; the terrain is much smoother than that of the high relief areas. The urban area is Numazu city, an industrial center.

We average the correlation value in each rectangular area. Figure 7a shows the relationship

between the correlation and the spatial baseline B_{perp} (baseline component perpendicular to look direction [Rosen *et* al., 1996]). The correlation of the interferograms including the image 2/12/94 is rather low, because it snowed heavily on that day on the north of the Izu peninsula. The lines in Fig. 7a are empirical decorrelation functions obtained by fitting various functions to the data neglecting [4/10/93-2/12/94] and [2/25/93-2/1 2/94] because of the snow decorrelation. For the city area and the forest area, the decorrelation is roughly linear with baseline length, with slopes close to the theoretical decorrelation function [*Zebker and Villasenor, 1992],* which is calculated from the critical baseline. At B_{perp}=0, the correlation is significantly below 1 because the decorrelation includes thermal noise and temporal decorrelation, independent of the spatial baseline. However, from Fig. 7a, the spatial baseline decorrelation is the dominant variable source of decorrelation in the city area.

In contrast, in the high relief areas, a linear function cannot be fitted to the decorrelation. Since the correlation rapidly increases when the spatial baseline goes to zero, the decorrelation function seems to be a power function, such as the broken line shown in Fig. 7a.

We normalize the correlation by the baseline correlation using the fitted lines in Fig. 7a. Figure 7b shows the adjusted correlation, as a function of temporal baselines. The correlation in the city area is stable and has very little relation to the temporal baseline. On the other hand, the correlation in the forest and the high relief areas shows greater variance and a slightly larger dependence on the temporal baseline than in the city area. The decorrelation includes temporal effects such as changing vegetation (growth, leaf fall, wind effects) and changing surface condition (soil moisture, freezing). Note that some of

the increased scatter in Fig 7b relative to Fig 7a, and particularly the correlation values exceeding 1, are due to imperfect estimates of the normalizing baseline correlation.

Two important points follow from the correlation curves in Fig. 7. First, it is evident that the forested area in the gentle slopes of Mt. Fuji obeys the same linear relationship to baseline as in the urban area, however, the basic level of correlation at zero baseline is lower. If there existed a significant variability of the decorrelation with time, we would not expect the linear relationship in Fig. 7a to hold. Therefore, we conclude that the forest, consisting of mixed conifer and deciduous trees in full leaf, decorrelates by a constant amount determined by the intrinsic random variability of the leaves and branches, but shows very small change over time. Second, the decor-relation in the high relief areas is most likely due to the combination of the time invariant temporal decorrelation described above and of local slope related effects. Recall that, though the topographic fringes have been removed from the interferogram before the correlation computation, the intrinsic area of each pixel projected into the look direction varies with topography. This leads to variability in the. critical baseline associated with each pixel, hence variability in the correlation from pixel to pixel, even for a fixed interferometric baseline. Conversely, from an area with a particular unchanging topography, the net correlation will decay rapidly with baseline length when slopes are high and more slowly when slopes are gentle. In particular, if slopes approach the look angle in the region, the real correlation will drop dramatically for all baselines longer than zero. This effect is apparent in Fig. 7a. Slopes in this area easily reach the JERS 1 look angle and high slope areas behave differently in correlation from low slope areas. The tapering of decorrelation with increasing baseline is a consequence of saturation of the slope effects, in this case: so much of the area contains high slopes that these correlations become zero immediately. The valley floors, however,

decorrelate at the usual flat surface rate.

Though L-band is more robust than C-band for minimizing effects of temporal decorrelation, the effect of wet snow cover is still large. The snowfall accumulated to more than 20 centimeters on February 12, 1994, in the northern part of the image. Numazu city was also covered with several cm of snow. The temperature in lowland areas was higher than 0° C [*Japan Meteorological Agency*, 1994] and the snow was probably quite wet, so the correlation of the wet snow area was low. Interestingly, however, the fringe risibilities of [2/25/93-2/12/94] (Plate 2c) and [4/10/93-2/12/94] (Plate 2h) are not as poor as one might expect. Evidently, the dominant scatterers in the resolution cells remained intact despite snow cover: building comers and tree branches will have unchanged scattering centers.

Zebker et al. [1994a] found in C-band ERS 1 data that interferograms decorrelate above a constant altitude on volcanoes, possibly from elevation-dependent weather effects. Plate 3c [2/25/93-4/10/93] shows similar decorrelation in high altitude areas, the northwestern part of the image and the summit of Mt. Fuji. In the winter months, such high mountain areas are usually covered with snow. However, the correlation of high mountains near the northwestern edge in [8/20/93-11/16/93] (Plate 3b) shows discernible y higher values than those in the surrounding lower mountains. This is because there is no snow in the summer and the vegetation is sub-alpine flora and sparse in the high mountains. This small vegetation likely allowed for higher correlation than that in lower mountains with heavy vegetation.

Discussion

Averaging of interferograms for noise reduction

Since the interferograms in wet and complicated topographic regions contain large phase delay undulations due to atmospheric water vapor, it is difficult to detect cm level surface deformation from only one interferogram. As there are no data on the detailed distribution of water vapor for the present time, the phase delay cannot be corrected. However, if the phase delay of the water vapor is randomly distributed, we can reduce the noise by averaging multiple interferograms [*Zebker et al. 1997*]. When *n* independent interferograms are averaged, the random noise becomes statistically smaller by a factor of $\sqrt{n}$. Because the interferograms necessarily span different time intervals, care must be taken in averaging if the surface deformation varies with time.

Plate 4 shows the averages of four interferograms [2/25/93-2/12/94] (Plate 2c), [4/10/93 - 2/12/94] (Plate 2h), [7/7/93-11/16/93] (Plate 2k) and [8/20/93-11/16/93] (Plate 21), and two interferograms [2/25/93-2/12/94] (Plate 2c) and [8/20/93-1 1/1 6/93] (Plate 21). Averaged phase cross sections of the two interferograms are shown in Fig. 4. The crustal deformation around Ito city occurred continuously from September to December (Fig. 9)[*Geographical Survey Institute,* 1994a and 1994b]. From Fig. 9, the interferograms including the image taken on 11/16/93 seem to contain about 60 % of the total amount of the crustal deformation because the deformation varied with time. For precise determination of the deformation, the interferograms selected for averaging should include all the period of the crustal deformation. However, we were obliged to use the image taken on 11/16/93 because of the limited availability y of data.

We pay attention to select the images that have higher fringe visibility for averaging. Since only two SAR images acquired after the crustal deformation are available, the images

taken on 11/16/93 and 2/12/94 are repeatedly used in the average of four interferograms. As a result of averaging, the crustal deformation is clearly seen in Plate 4. However, the atmospheric phase delay still remains. The phase delays on shorter wavelength scales are larger in the average of two interferograms while the average of four looks very smooth, but the phase delays of longer wavelengths in the southern Izu peninsula are emphasized in the average of four interferograms. These long-scale changes were not found from other geodetic observations *[Geographical Survey Institute,* 1994a and 1994b]. This false emphasis must be caused by the images taken on 4/10/93 and 7/7/93. As shown in Fig. 6a, the atmospheric phase delay is larger at longer spatial wavelengths. Accordingly, when averaging, we should avoid using interferograms that have large atmospheric undulations at longer period.

To make further progress in quantitative comparisons with leveling data, we must scale the 11/16/93 interferogram's phase by 1.7 to emulate an observation that spans the entire deformation event, Figure 8a shows the radar line-of-sight displacements of the scaled average interferogram, and Fig. 8b shows the vertical uplift scaled by the cosine of the look angle of JERS 1 (equivalent to radar line-of-sight apparent displacement) found by precise leveling from summer 1993 to summer 1994 (after *[Geographical Survey Institute*, 1995]). Figure 8c shows the difference of Figs. 8a and 8b. Because the radar measures both vertical and horizontal displacements projected into the radar line of sight, the difference in Fig 8c represents the horizontal displacements in the radar direction around Ito city. Region A in Fig. 8c shows westward displacement and region B shows eastward displacement, each with magnitude of roughly 5-6 cm. No deformation north or south of the area is observed, either because there was no motion, or because the motion was perpendicular to the radar look direction. The residuals between radar and leveling data are 0.5 cm in the north (N

area in Fig.8c) and south (S area in Fig.8c), and 1.5 cm overall. The loop-closing accuracy of the leveling measurements is also of order 1 cm.

Figures 8b and 8C taken together strongly suggest balloon-like crustal inflation from a localized magma source at a depth of 5-10 km, with its center in between A and B in Fig. SC. The earthquakes in autumn 1993 occurred at a depth of about 5 km and a region of epicenters in October and November is shown in Fig. 2 *[Earthquake Prediction Information Division, 1994].* This region likely coincides with the region of the magma activity. The vertical dyke model of the 1989 event [*Okada and Yamamoto, 1991] does* not show this balloon-like crustal deformation. Magma flowing up through the crust at a low angle (as in a horizontal dyke) near Ito city possibly caused this signature. The ability to discriminate between source mechanisms is enhanced in this case by the radar observations relative to simply the sparse leveling data.

Conclusions

We have shown that JERS 1 SAR data can support radar interferometry applications to the measurement of surface topographic change, exhibiting remarkable consistency with the in situ measurements, in spite of non-negligible errors. Many of these errors can be more or less mitigated in future generations of L-band synthetic aperture radar satellites. Added transmit power will decrease thermal noise. Better orbit control will minimize baseline decorrelation, particularly in areas of high relief where correlation appears to decrease exponentially with increasing baseline. More frequent observations will allow interferogram averaging to decrease decorrelation effects and water vapor anomalies. Finally, synoptic simultaneous imagery of cloud cover may allow estimates of the water vapor variability in a given scene. With these observational enhancements, repeat-pass

interferometry will transform from data-intensive, site specific studies of signal and coincident noise effects to an operational tool for geodesy and geophysics. We are well on our way toward understanding the mechanisms and signatures of decorrelation in various types of terrain. With more data and symbiotic comparison to land cover maps, an information system can be built to take advantage of decorrelation signatures for land classification and change detection.

Appendix A: The influence of water vapor on baseline estimation

We use unwrapped phase to calculate precise baselines. Since we cannot distinguish atmospheric noise from signal in the phase, the estimated baselines will have errors. If the baseline estimate has an error, the interferogram may have a systematic distortion of the observed phase. As we assume that the repeat-pass baseline of JERS 1 is a linear function of the azimuth position of the satellite, the phase delay that has much shorter wavelength than the azimuth image size (in this study 140 km) will not affect the baseline estimation because we average these random variations over the images. However, we cannot avoid longer wavelength effects, which are likely larger than the azimuth image size. The only way to cancel their influence is to estimate the long wavelength phase delay using an independent method such as three-dimensional numerical weather modeling [*Ichikawa et al., 1995]* or a dense array of GPS stations from which zenith delay can be estimated regularly. If we cannot estimate this delay, we should use as large SAR images as possible and should not rely on the inferred deformation at the longest wavelength. In addition, we can average interferograms to minimize the error.

Appendix B: For DEM production

When the baseline is smaller (< 100 m), the fringe visibility is better even in high relief areas, and we can unwrap the phase. Though it is better to maximize the baseline within the limit of decorrelation [*Zebker et al., 1997],* that limit in high relief areas is too low to make a high precision DEM. Therefore, the large decorrelation in the high relief areas and the large undulation of the atmospheric delay prevent us from making a high precision DEM throughout the image in this study using JERS 1 interferometry. To create a good DEM in this region, we will need to average results from a large number of interferograms with short baselines (several tens of meters). Moreover, tighter control and knowledge of interferometric baselines would greatly enhance the mechanics of DEM production. Though it is possible to make a good DEM from only one interferogram in a drier region with smoother topography such as Northern Sakhalin [*Tobita et al,* 1997], it would be difficult in most tectonically active areas, which have high relief.

Acknowledgments.

The JERS 1 SAR data used in this study were provided by NASDA through Remote Sensing Technology Center of Japan (RESTEC). Ministry of International Trade and Industry of Japan (MITI) and NASDA retain the ownership of the original data. We thank to MITI/NASDA and RESTEC for providing the data. We wish to thank the Science and Technology Agency of Japan for financial support for two of the authors (S. Fujiwara and M. Tobita). We are grateful to Scott Hensley and Charles L Werner of JPL for supporting the analyses, and members of the GSI for their assistance in collecting the data and the materials. Reviewers Timothy Dixon and Jean-Bernard Minster and JGR associate editor Joseph Engeln greatly improved the manuscript in form and content.

References

Dixon, T. H., and S. K. Wolf, Some tests of wet troposphere calibration for the CASA UNO Global Positioning System experiment, *Geophys. Res. Lett.*, *17.203-206,* **1990.**

Earthquake Prediction Information Division, Japan Meteorological Agency. Seismic activity in and around the Izu Peninsula (May-October, 1993), *Report of the coordinating committee for earthquake prediction,* edited by Geographical Survey Institute, 51,292-309, 1994.

Fielding, E., S. Fujiwara, S. Hensley, P. A. Rosen, M. Tobita, and M. Shimada, Surface deformation due to the May 27, 1995 Sakhalin earthquake and related events measured by JERS-1 SAR interferometry, *Eos Trans. AGU*, 77, Fall Meet. Suppl., F36, 1996.

Geographical Survey Institute, Crustal movements in the Izu Peninsula and its vicinity, *Report of the coordinating committee for earthquake prediction,* edited by Geographical Survey Institute, 51,373-400, 1994a.

Geographical Survey Institute, Crustal movements in the Izu Peninsula and its vicinity, *Report of the coordinating committee for earthquake prediction,* edited by Geographical Survey Institute, 52,272-290, 1994b.

Geographical Survey Institute, Crustal movements in the Izu Peninsula and its vicinity, *Report of the coordinating committee for earthquake prediction,* edited by Geographical Survey Institute, 53,356-375,1995.

Goldstein, R. M., H. A. Zebker, and C. L. Werner, Satellite radar interferometry: Two-dimensional phase unwrapping, *Radio Sci., 23,713-720,1988.*

Goldstein, R. M., Atmospheric limitations to repeat-track radar interferometry, *Geophys. Res. Lett., 22,2517-2520, 1995.*

Herring, T. A., Precision of vertical position estimates from very long baseline

interferometry, *J. Geophys. Res., 91, 9177-9182,* **1986.**

Ichikawa, R., M. Kasahara, N. Mannoji, and I. Naito, Estimations of atmospheric excess path delay based on three-dimensional, numerical prediction model data, *J. Geodetic Society Japan,* 41,379-408, 1995.

Japan Meteorological Agency, *Monthly report,* Japan Meteorological Agency, published monthly, 1993 and 1994.

Massonnet, D., M. Rossi, C. Carmona, F. Adragna, G. Peltzer, K. Fiegl, and T. Rabaute, The displacement field of the Landers earthquake mapped by radar interferometry, *Nature, 364, 138-142, 1993.*

Massonnet, D., P. Briole, and A. Amaud, Deflation of Mount Etna monitored by spaceborne radar interferometry, *Nature, 375, 567-570, 1995.*

Murakami, Mak., S. Fujiwara, and T. Saito, Detection of crustal deformations associated with the 1995 Hyogo-ken-nanbu earthquake by interferometric SAR, *Biannual Rep. Geograph. Surv. Inst., 83,24-27,1995* (in Japanese).

Murakami, Mak., M. Tobita, S. Fujiwara, T. Saito, and H. Masaharu, Coseismic crustal deformations of 1994 Northridge, California, earthquake detected by interferomet ric JERS 1 synthetic aperture radar, *J. Geophys. Res., 101,* 8605-8614, 1996a.

Murakami, Mas., M. Tobita, H. Nakagawa, K. Nitta, Mak. Murakami, M. Shimada, H. Oaku, K Isono, P. A. Rosen, and S. Fujiwara, Crustal deformations associated with 1995 Neftegorsk, Northern Sakhalin, earthquake detected by JERS-1/SAR interferometry, *Programs and Abstracts*, 86th meeting Geodetic Sot. Japan, 117-118, 1996b.

Okada, Y., and E. Yamamoto, Dyke intrusion model for the 1989 seismovolcanic activity off Ito, central Japan, *J. Geophys. Res.,* 96, 10,361-10,376, 1991.

Peltzer, G., and P. A. Rosen, Surface displacement of the 17 May 1993 Eureka Valley. California, earthquake observed by SAR interferometry, *Science,* 268, 1333-1336, 1995.

Rosen, P. A., S. Hensley, H. A. Zebker, F. H. Webb, and E. J. Fielding, Surface deformation and coherence measurements of Kilauea volcano, Hawaii, from SIR-C radar interferometry, *J. Geophys. Res., 101,* 23,109-23,125, 1996.

Rossi, M., B. Rogron, and D. Massonnet, JERS-1 SAR image quality and interferometric potential, *IEEE Trans. Geosci. Remote Sens., 34,824-827,1996.*

Shimada, M., M. Nakai, and S. Kawase, Inflight evaluation of the L-band SAR of JERS-1, *Can. J. Remote Sens., 19,247-258,1993.*

Shimoyama, Y., S. Iida, K. Kawase, and H. Matsumoto, Verification of the 50m grid DEM data's accuracy, *Biannual Rep. Geograph. Surv. Inst., 84, 64-72,1995* (in Japanese).

Tada, T., and M. Hashimoto, Anomalous crustal deformation in the northeastern Izu Peninsula and its tectonic significance – tension crack model -, *J. Phys. Earth, 39,* 197-218,1991.

Tobita, M., S. Fujiwara, S. Ozawa, Mas. Murakami, H. Nakagawa, K. Nitta, Mak. Murakami, and P. A. Rosen, Deformation of 1995 North Sakhalin earthquake detected by JERS-1/SAR Interferometry, *in preparation, 1997.*

Wegmüller U., and C. L. Werner, SAR interferometric signatures of forest, *IEEE Geosci. Remote Sens., 33,1153-1161,1995.*

Zebker, H. A., and J. Villasenor, Decorrelation in interferometric radar echoes, *IEEE Trans. Geosci. Remote Sens., 30,950-959,1992.*

Zebker, H. A., C. L. Werner, P. A. Rosen, and S. Hensley, Accuracy of topographic maps derived from ERS-1 inter ferometric radar, *IEEE Trans. Geosci. Remote Sens., 32,*

823-836, 1994a.

Zebker, H. A., P. A. Rosen, R. M. Goldstein, A. Gabriel, and C. L. Werner, On the derivation of coseismic displacement fields using differential radar interferometry: The Landars earthquake, *J. Geophys. Res.,* 99, 19,617-19,634, 1994b.

Zebker, H. A., P. A. Rosen, S. Hensley, and P. J. Mouginis-Mark, Analysis of active lava flows on Kilauea volcano, Hawaii, using SIR-C radar correlation measurements, Geology, 24,495-498, 1996.

Zebker, H. A., P. A. Rosen, and S. Hensley, Atmospheric artifacts in interferometric SAR surface deformation and topographic maps, *J. Geophys. Res., 102, 7547-7564,* 1997.

Figure captions:

Plate 1. JERS 1 interferogram of [8/20/93-11/16/93]. One cycle of interferometric phase change is shown as the color wheel. One cycle of the phase change corresponds to 11.8 cm changes in range and 260 m of topographic variation.

Plate 2a. An example of simulated topographic interferogram using a DEM.

b-1. Differential interferograms from which the simulated topographic phase is removed. Because of the decorrelation, we cannot unwrap the phase of some interferograms. Therefore, phase unwrapping is not applied here. A positive phase change (blue to red to yellow to green) corresponds to an increase in the range. Spatial baseline B_{perp} (m) and temporal baseline (days) are shown in each interferogram (bottom right).

Plate 3. Correlation maps corresponding to best (c)[2/25/93-4/10/93] (Plate 2b), average (b)[8/20/93-11/16/93] (Plate 21) and worst (a)[4/10/93-8/20/93] (Plate 2e) cases.

Plate 4. Averaged interferograms. The left (a) is the average of four images [2/25/93-2/12/94] (Plate 2c), [4/10/93-2/12/94] (Plate 2h), [7/7/93-11/16/93] (Plate 2k) and [8/20/93-11/16/93] (Plate 21), and the right (b) is that of two images [2/25/93-2/12/94] (Plate 2c) and [8/20/93-11/16/93] (Plate 21). Phase unwrapping is applied to each image.

Figure 1. Map of Japan showing the area imaged in this study. Tectonic plates and their boundaries are shown (PH: the Philippine Sea plate, NA: North American plate, EU: Eurasian plate, PA: Pacific plate).

Figure 2. JERS 1 SAR backscatter amplitude map. Rectangles show areas where we calculate correlation coefficients in Fig. 7a and 7b. Interferometric phase cross sections along A-B, C-D and G-H are shown in Figs. 4, 3 and 5, respectively. Lines E and F show mountain ridges which are border lines of weather effects in some interferograms. An ellipse shows a region of epicenters in October and November 1993 (after *[Earthquake Prediction Information Division,* 1994]). A star shows an epicenter of the 1978 Izu-Oshima-Kinkai earthquake (M=7.0).

Figure 3. Horizontal cross section of the phase delay along line C-D shown in Fig. 2. A low-pass filter is applied to the cross section data.

Figure 4. Horizontal cross section of the phase delay along line A-B shown in Fig. 2. A low-pass filter is applied to the cross section data. Average line shows an average of two cross sections [2/25/93-2/12/94] (Plate 2c) and [8/20/93-1 1/16/93] (Plate 2 1) .

Figure 5. Horizontal cross section of the phase delay [8/20/93-11/16/93] (Plate 21) and topography along line G-H shown in Fig. 2. A low-pass filter is applied to the cross section data.

Figure 6a. Power spectra of the phase delay along line A-B shown in Fig. 2. Added lines are fitted to the data using the least square method. Broken lines show 8/3 power slope.

b. Daily mean of cloud cover average at Kofu and Irozaki, versus power of phase

delay at 1 km wavelength in Fig. 6a.

Figure 7a. Correlation coefficients in areas shown in Fig.2 as a function of spatial baseline B_{perp} (baseline component perpendicular to the look direction).

b. Correlation coefficients normalized for the effect of the spatial baseline B_{perp}, using the fitted functions in Fig. 7a, as a function of temporal baseline.

Figure 8a. Radar line-of-sight apparent displacement (cm) in averaged interferogram of two images [2/25/93 -2/12/94] (scaled by 1.0) and [8/20/93-11/16/93] (scaled by 1.7). A positive number corresponds to a decrease in the range, which is uplift or eastward displacement.

b. Vertical uplift scaled by the cosine of the look angle of JERS 1 (equivalent to radar line-of-sight apparent displacement) measured by precise leveling from summer 1993 to summer 1994 (after *[Geographical Survey Institute*, 1995]). Black squares show the benchmarks. Contour lines are plotted by interpolating the data. A positive number corresponds to a decrease in the range, which is uplift displacement.

c. Difference of 8a and 8b. The residuals between radar and leveling data are 0.54 cm in N area, 0.53 cm in S area and 1.53 cm overall.

Figure 9. Uplift measured by GPS continuous observations around Ito in 1993 and 1994 and observation sites (after *[Geographical Survey Institute*, 1994a and 1994b]).

Table 1. Dates of JERS 1 data acquisition used in this study. The data acquisition time is

about 10 o'clock of local time for all data. Daily mean of cloud cover at Kofu and Irozaki (locations are shown in Fig. 2), daily precipitation and vapor pressure on the day of the JERS 1 data acquisition are shown (after [*Japan Meteorological Agency*, 1993 and 1994]). The cloud cover scale runs from O to 10, where 10 is complete coverage.

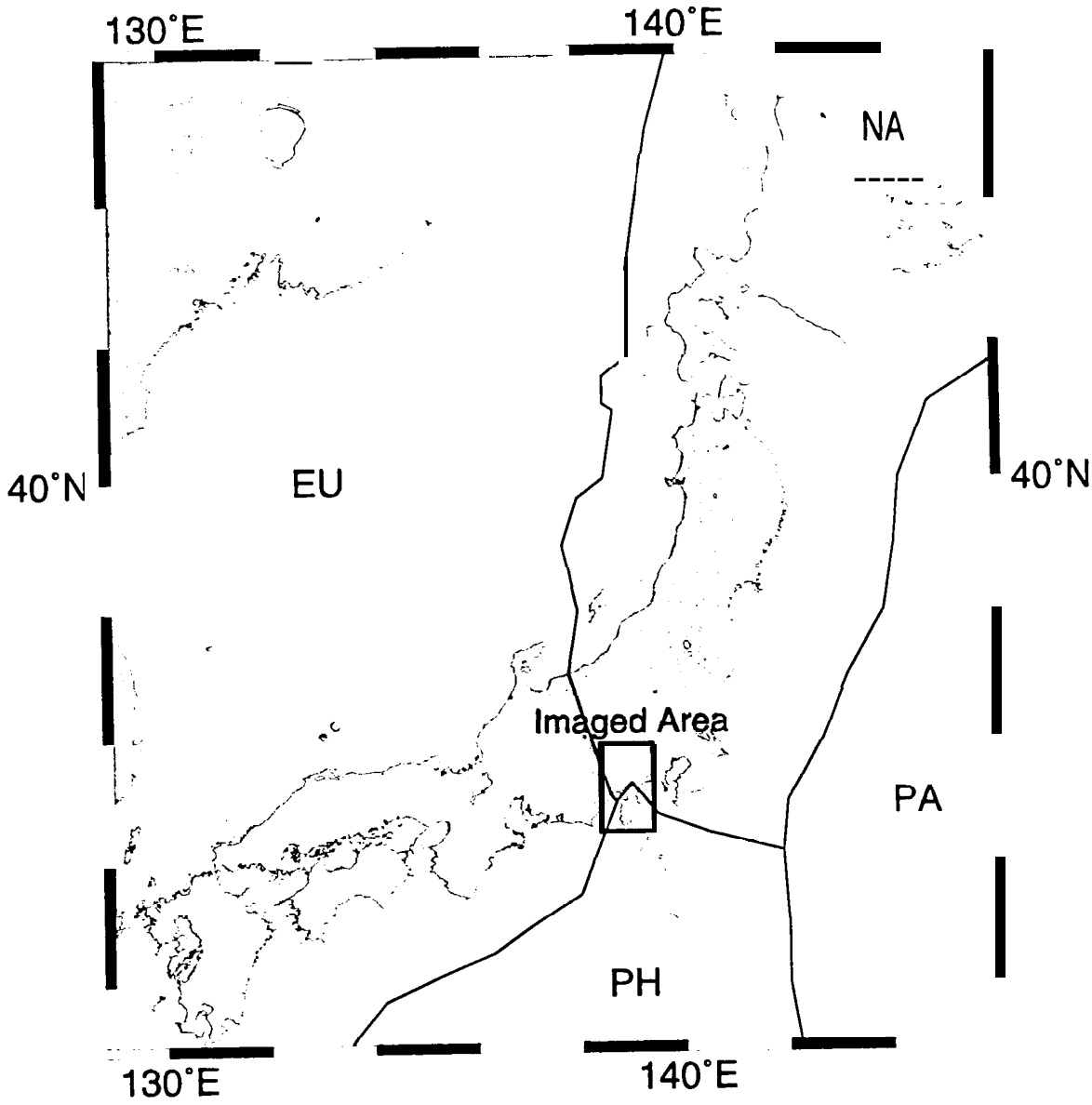

Figure 1 Fujiwara et al., 1997

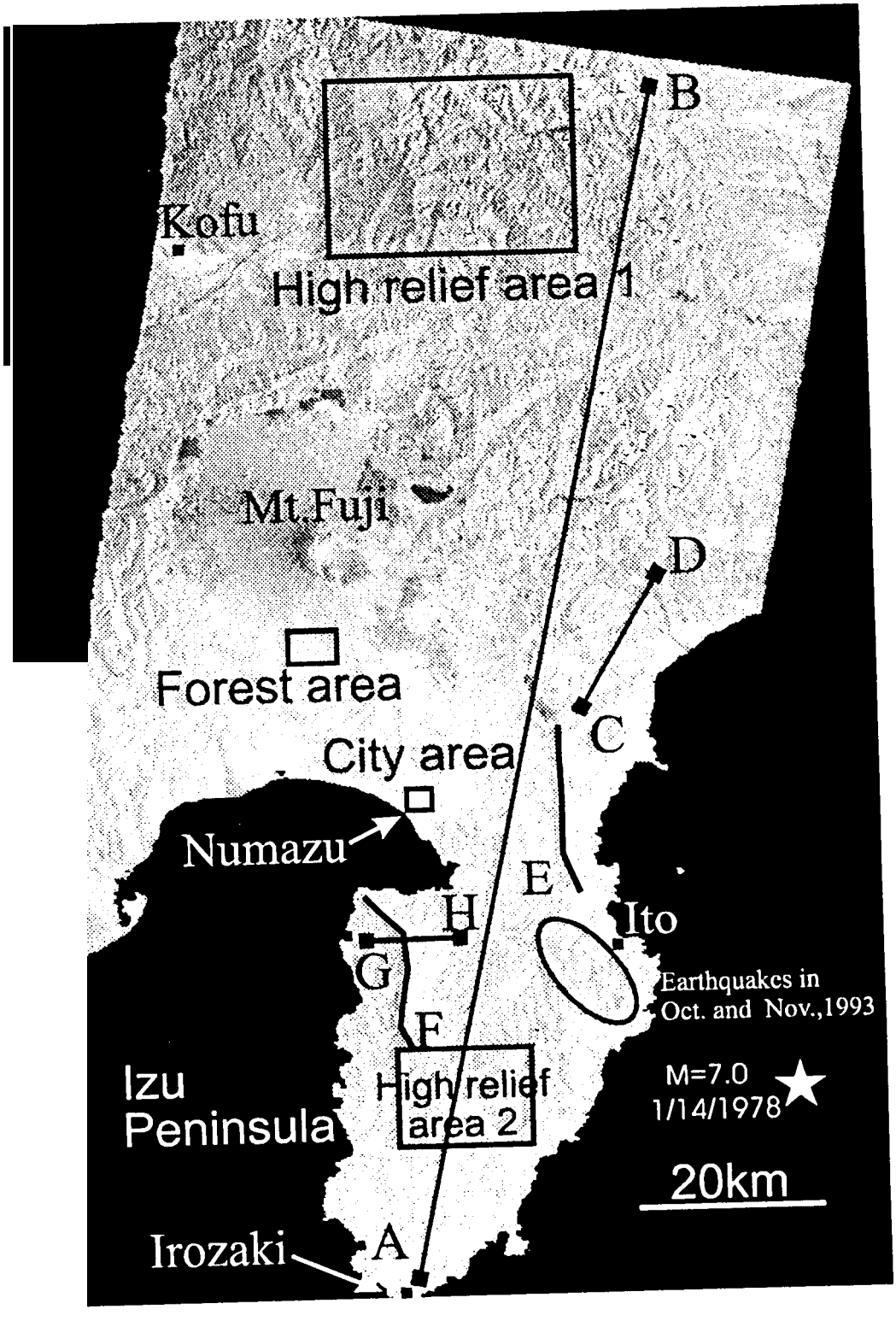

Figure 2 **Fujiwara** et al., 1997

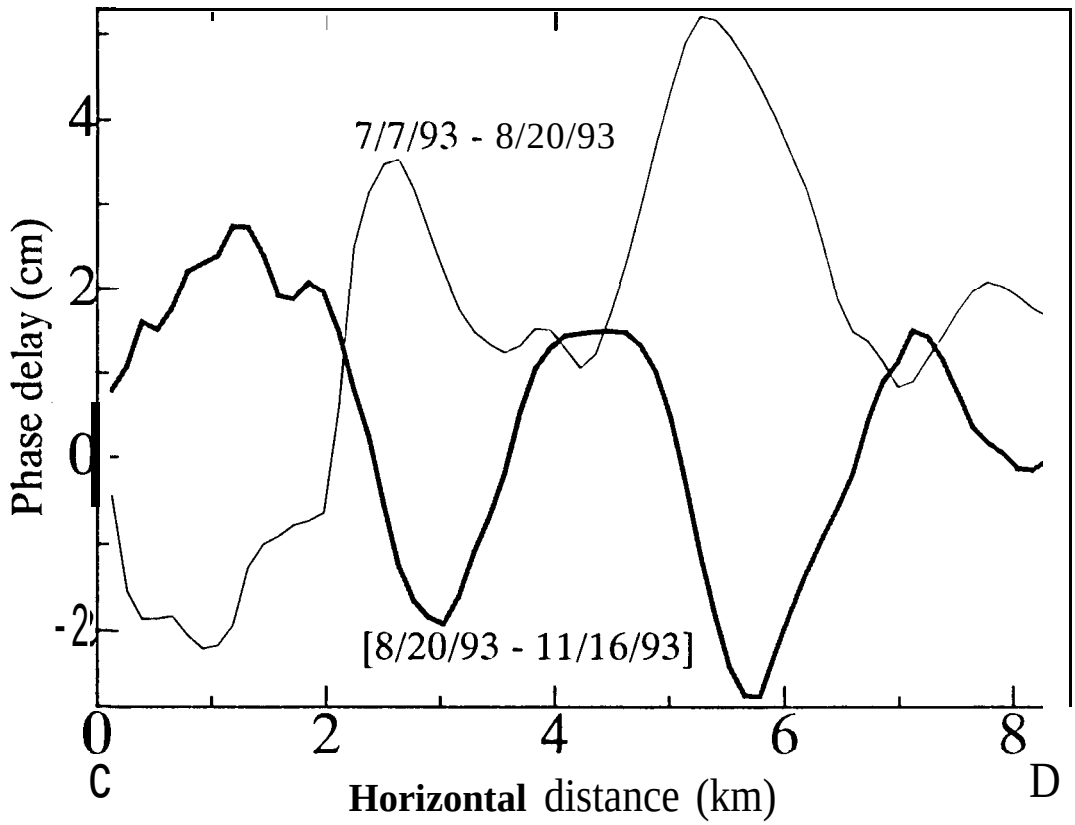

Figure 3 **Fujiwara** et al., 1997

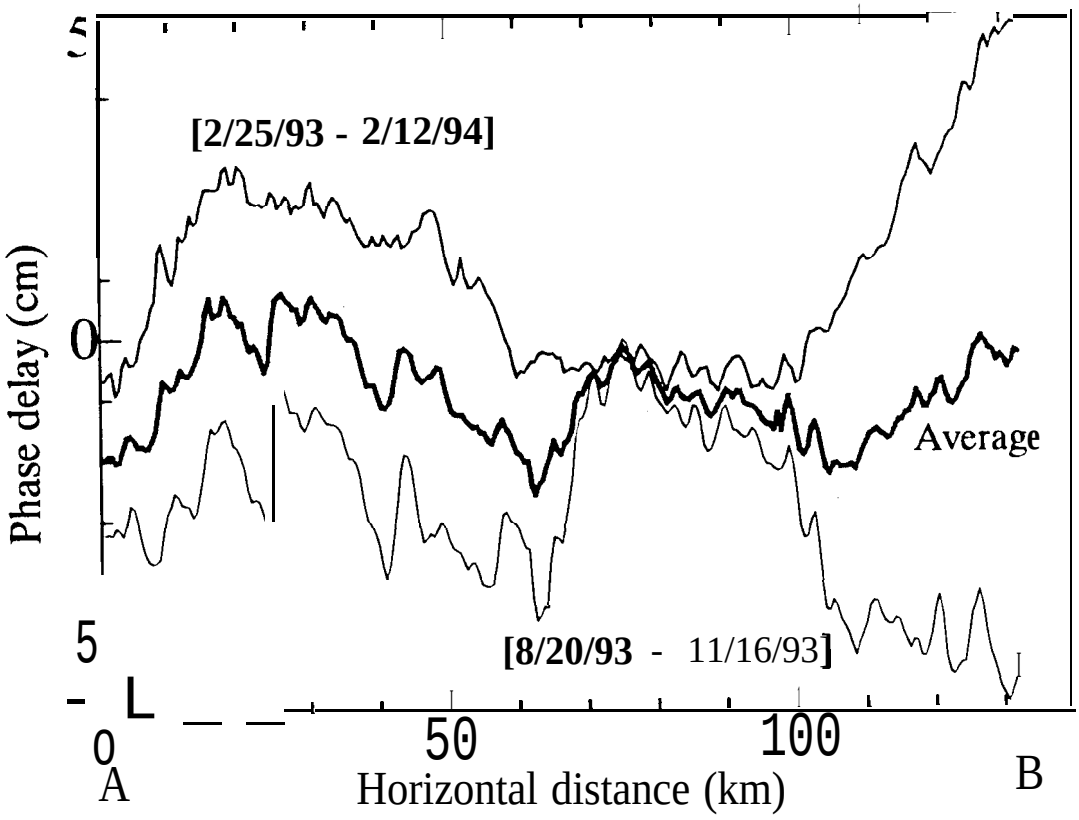

Figure 4 Fujiwara et al., 1997

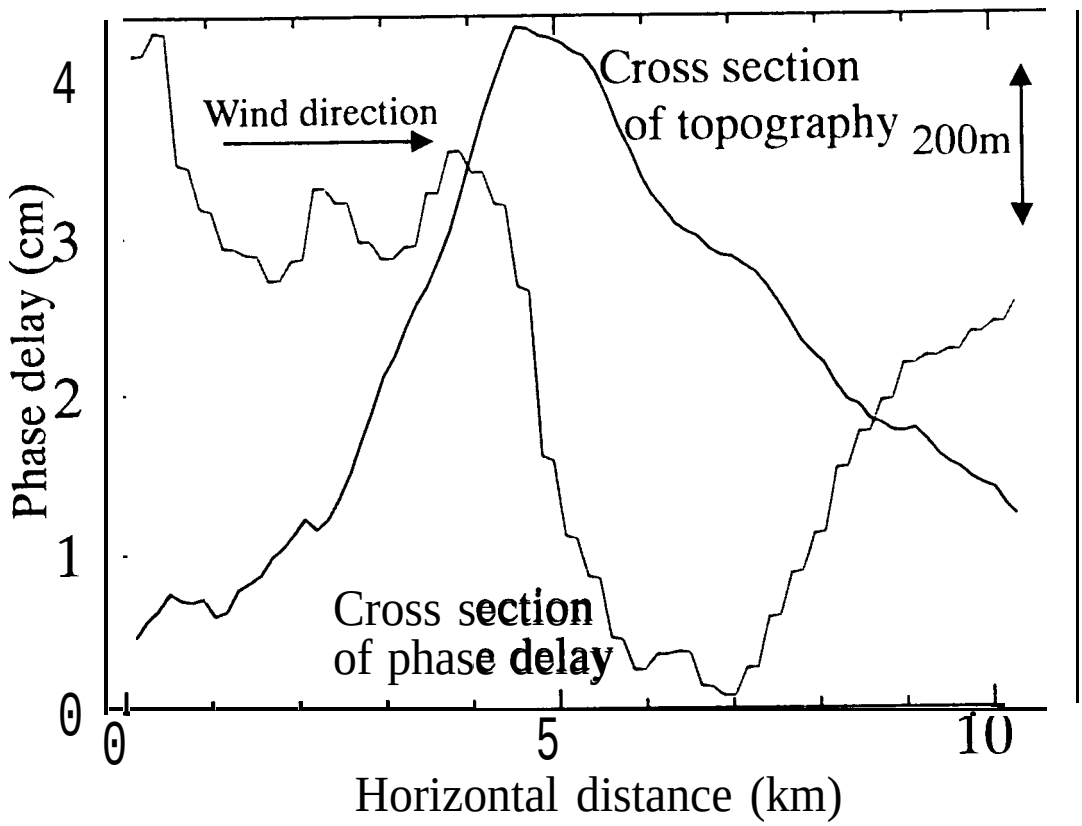

Figure 5 Fujiwara et al., 1997

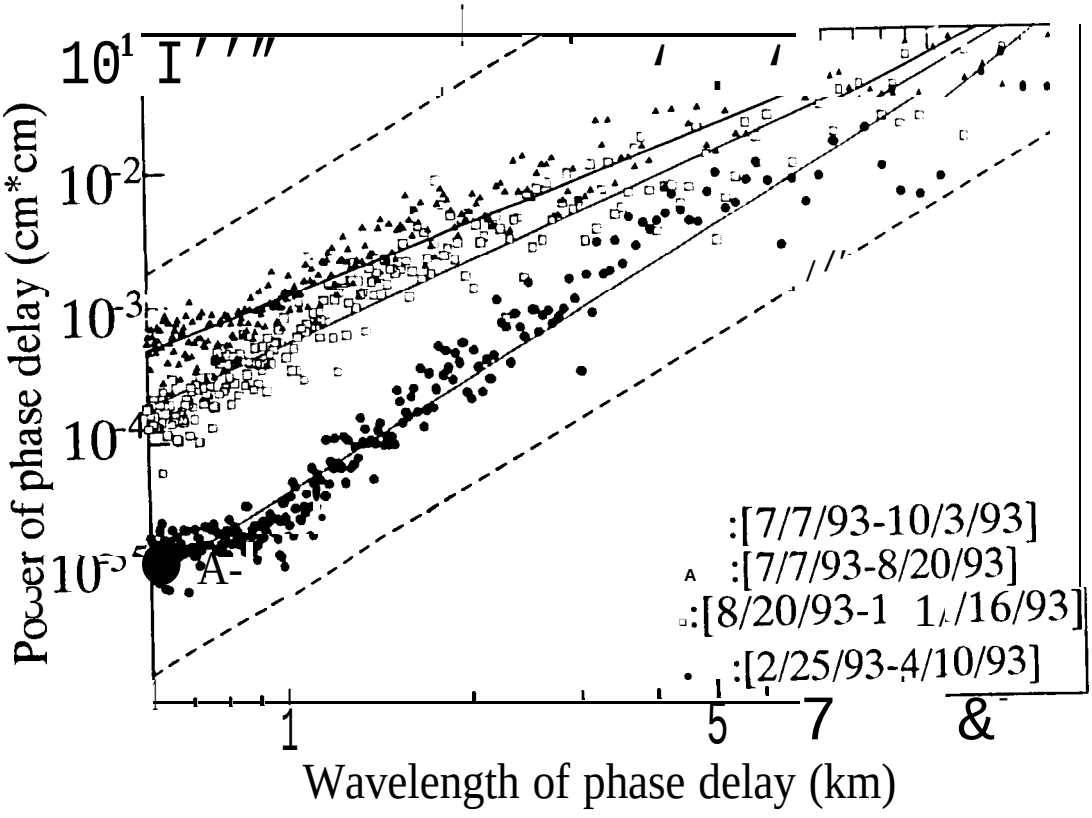

Figure 6a Fujiwara et al., 1997

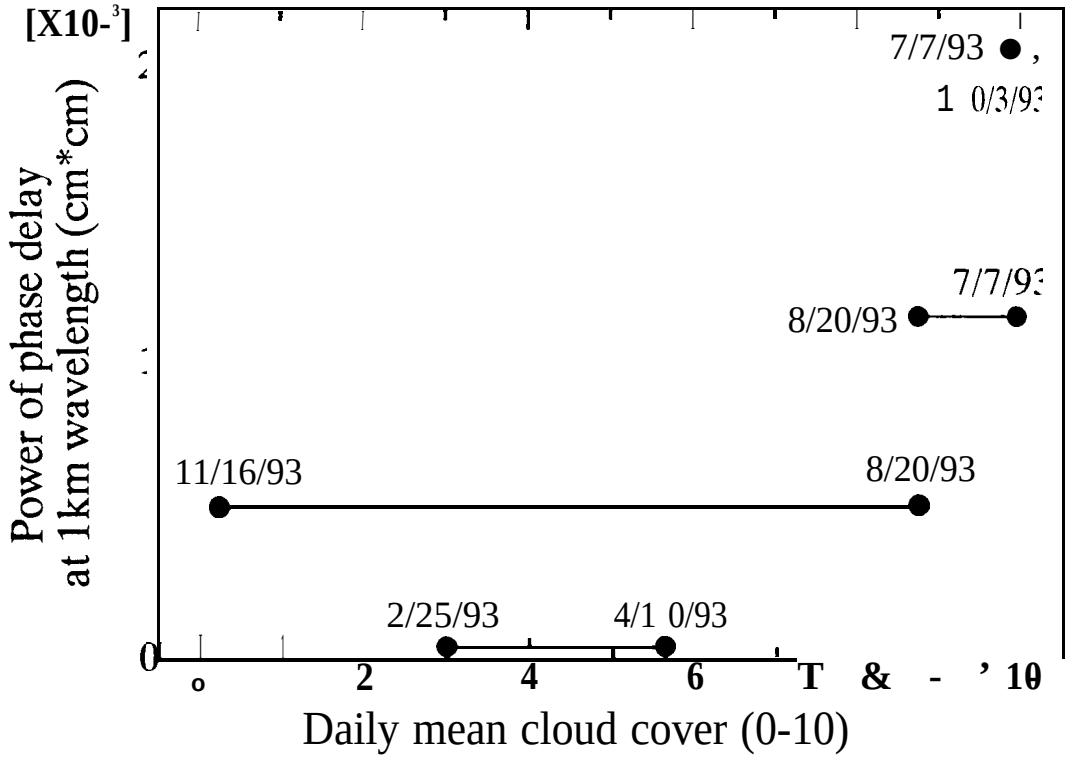

Figure 6b **Fujiwara** et al., 1997

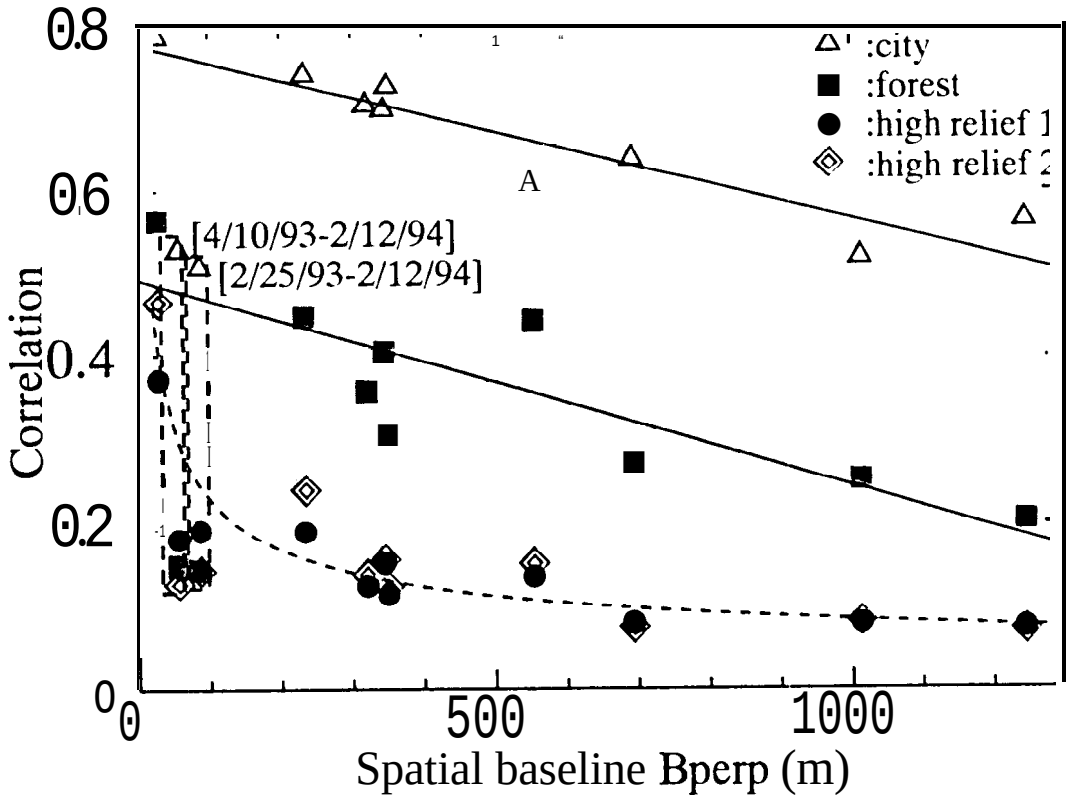

Figure 7a **Fujiwara** et al. , 1997

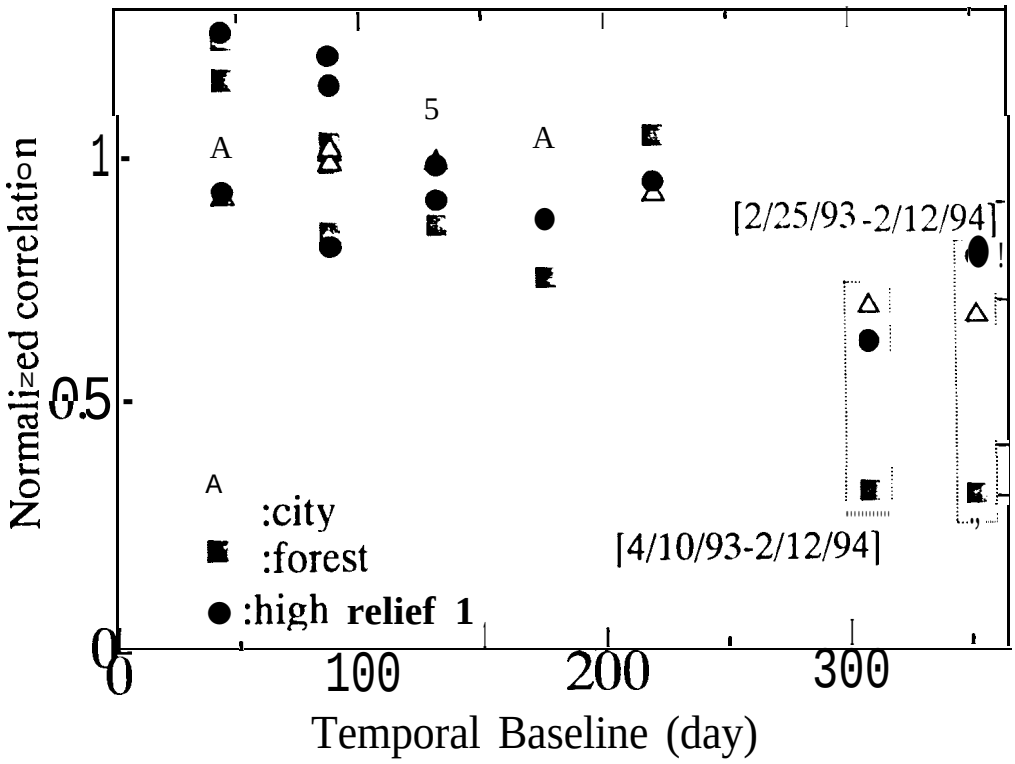

Figure 7b Fujiwara et al. , 1997

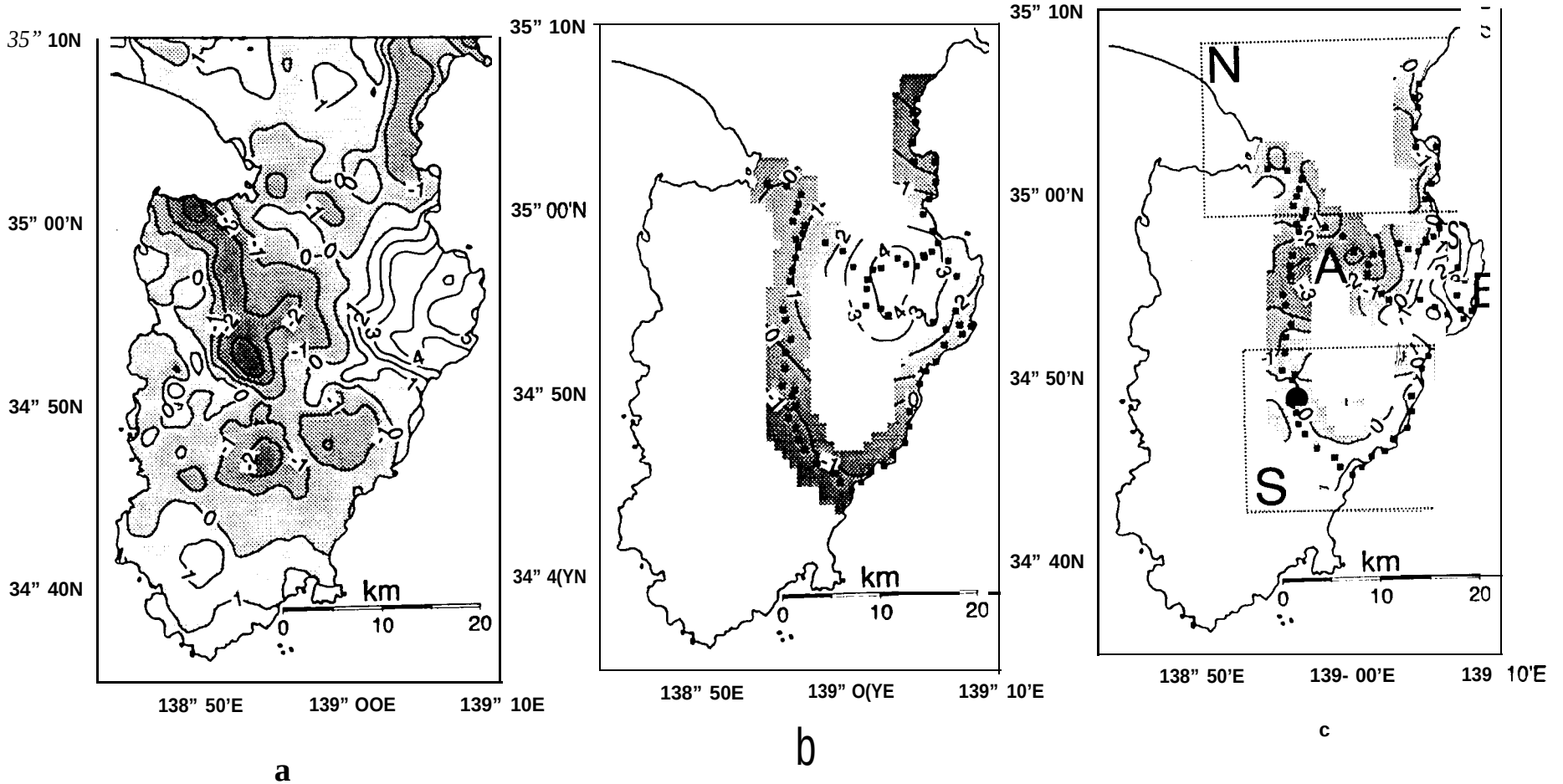

Figure 8 Fujiwara et al., 1997

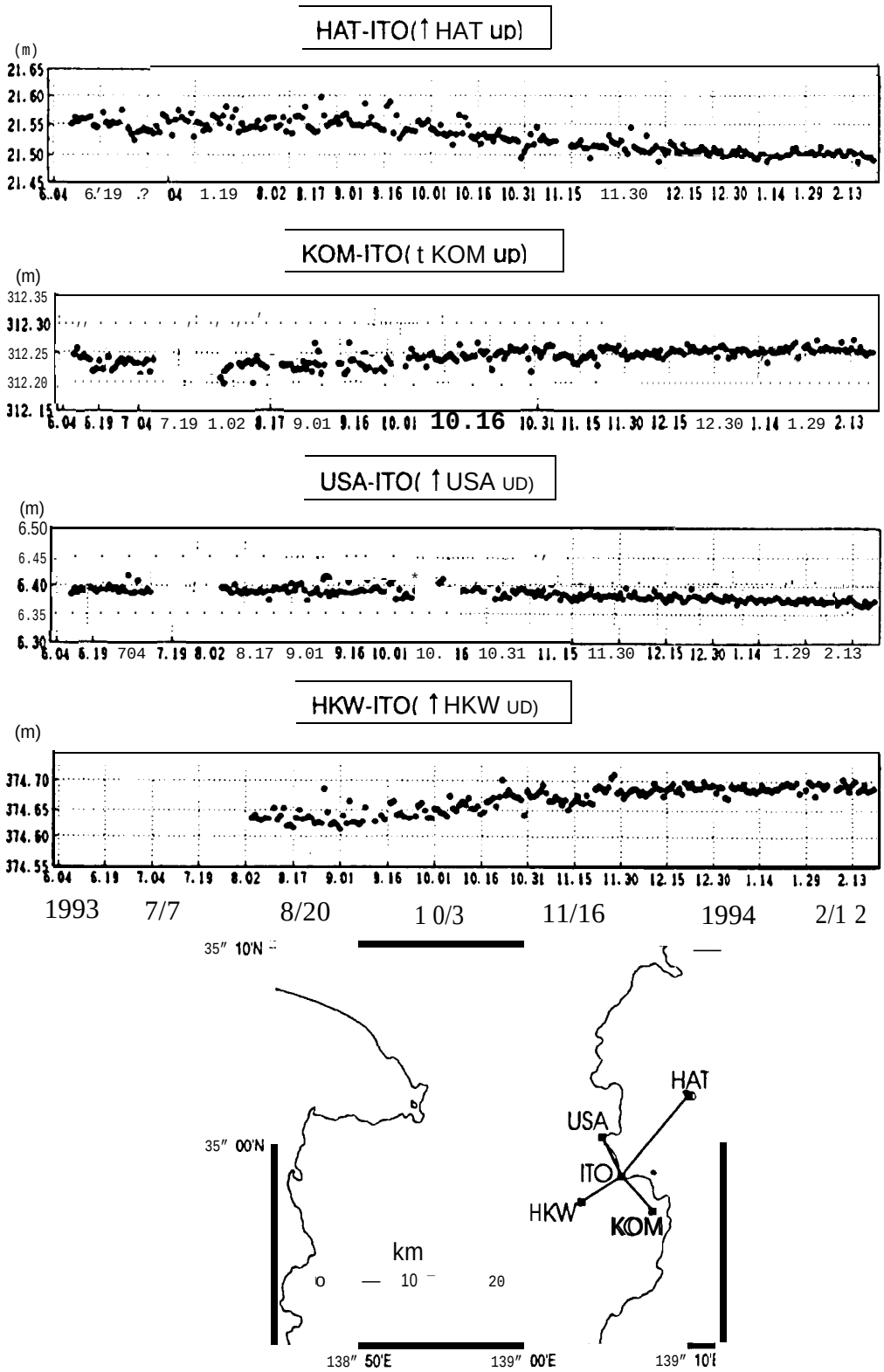

Figure 9 Fujiwara et al. , 1997

Table 1 **Fujiwara** et al., 1997

date (44 days interval)	Kofu				Irozaki			
	weather	precipitation (mm)	vapor pressure (hPa)	cloud cover (o-lo)	weather	precipitation (mm)	vapor pressure (hPa)	cloud cover (o-lo)
2/25/1993	sunny	0.0	2.7	0.0	fair	0.0	4.9	6.0
4/10/1993	partly cloudy	0.0	4.0	1.8	mostly cloudy	0.0	6.6	9.s
*								
7/7/1993	cloudy	5.0	18.9	9.5	rain	13.0	19.2	10.0
8/20/1993	cloudy	3.5	25.8	7.5	cloudy	0.0	29.9	10.0
10/3/1993	rain	16.0	14.1	10.0	rain	33.5	15.7	10.0
11/16/1993	sunny	0.0	9.4	0.0	sunny	0.0	14.0	0.5
*								
2112/1994	snow	20.5	4.5	9.5	sleet, wind	23.0	6.9	10.0

* no data available

Plate 1 Fujiwara et al., 1997

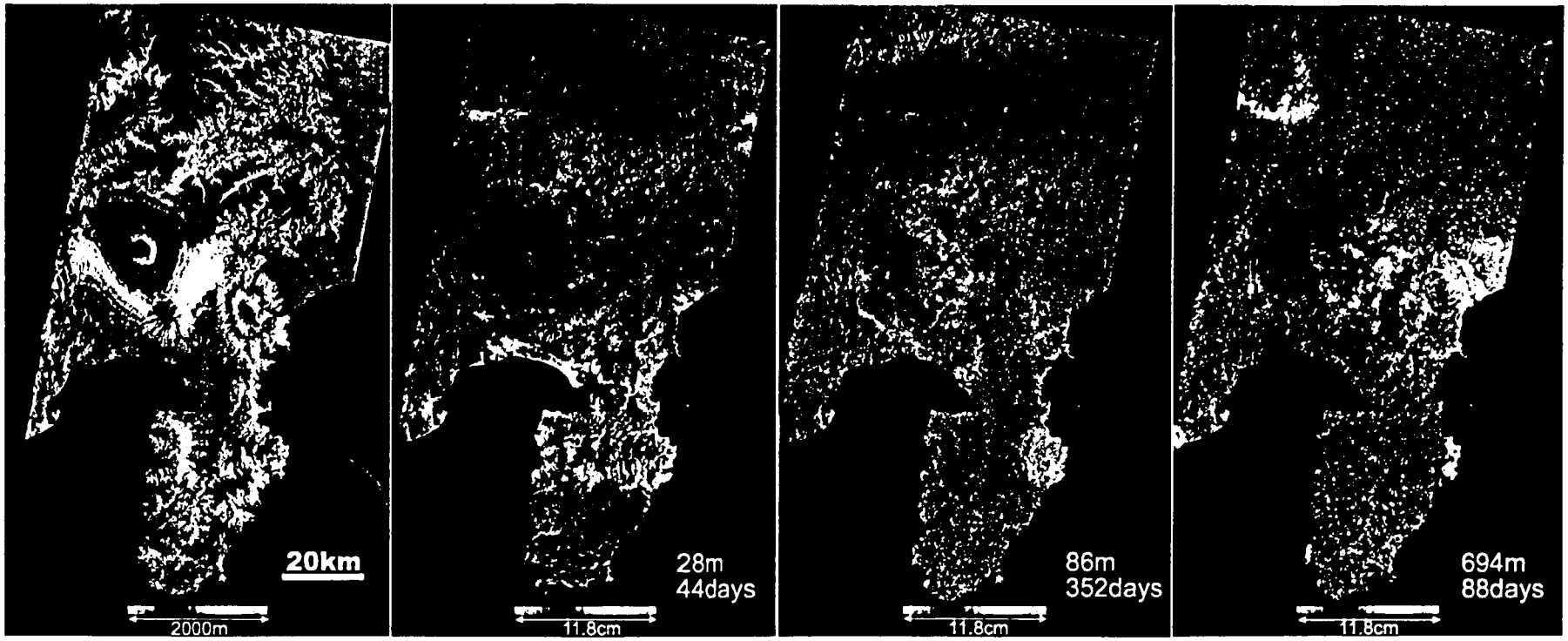

(a) Simulation Image (b) **[2/25/93-4/10/93]** (C) **[2/25/93-2/12/94]** **(d) [4/10/93-7/7/93]**

Plate 2a-2d Fujiwara et al., 1997

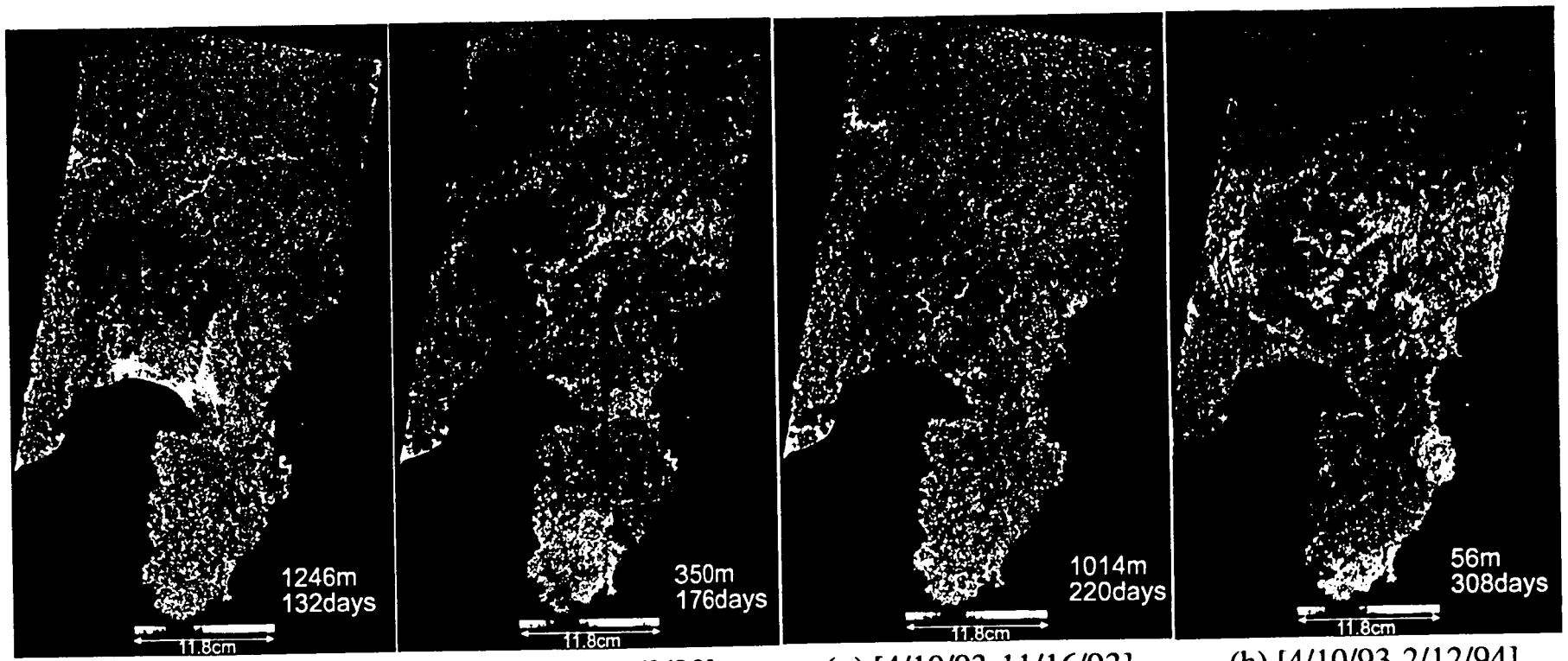

(e) [4/10/93-8/20/93] (f) [4/10/93-10/3/93] (g) [4/10/93-11/16/93] (h) [4/10/93-2/12/94]

Plate 2e-2h Fujiwara et al., 1997

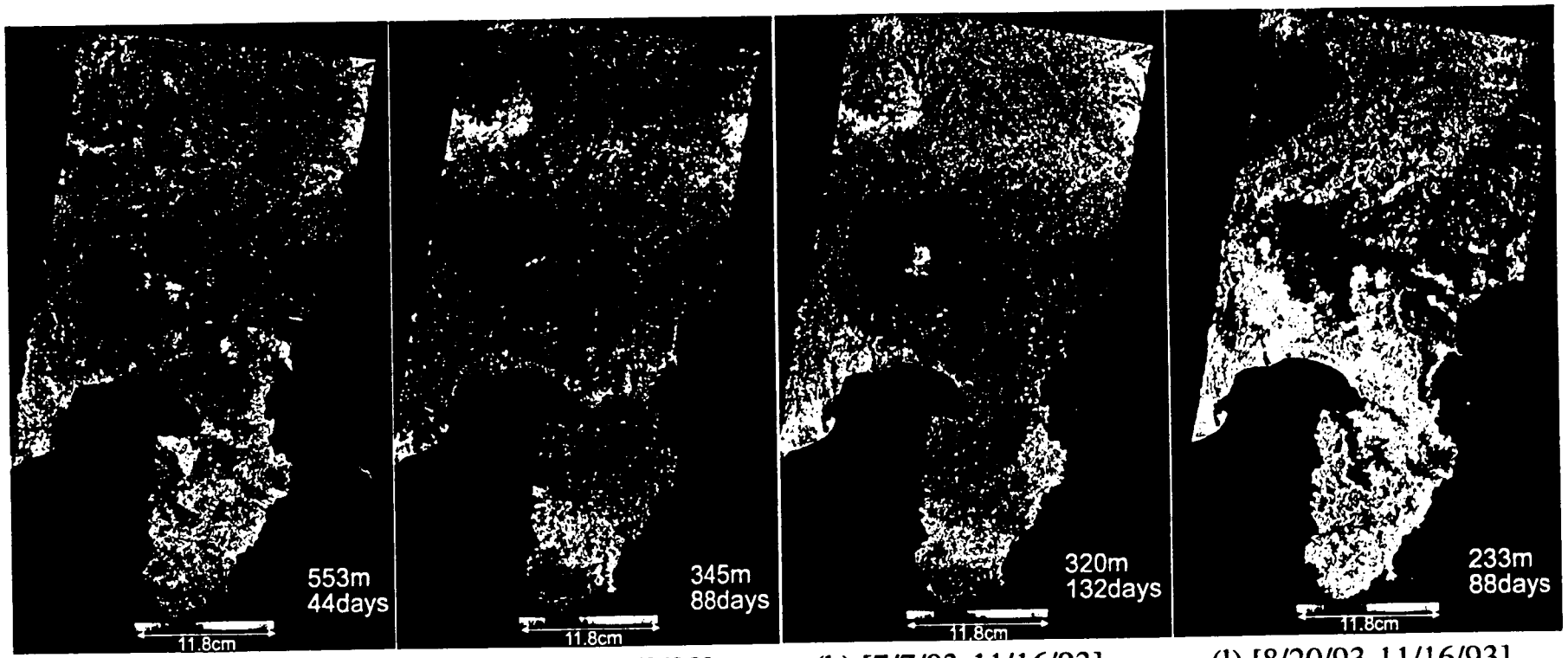

(i) [7/7/93-8/20/93] (j) [7/7/93-10/3/93] (k) [7/7/93-11/16/93] (l) [8/20/93-11/16/93]

Plate 2i-2l Fujiwara et al., 1997

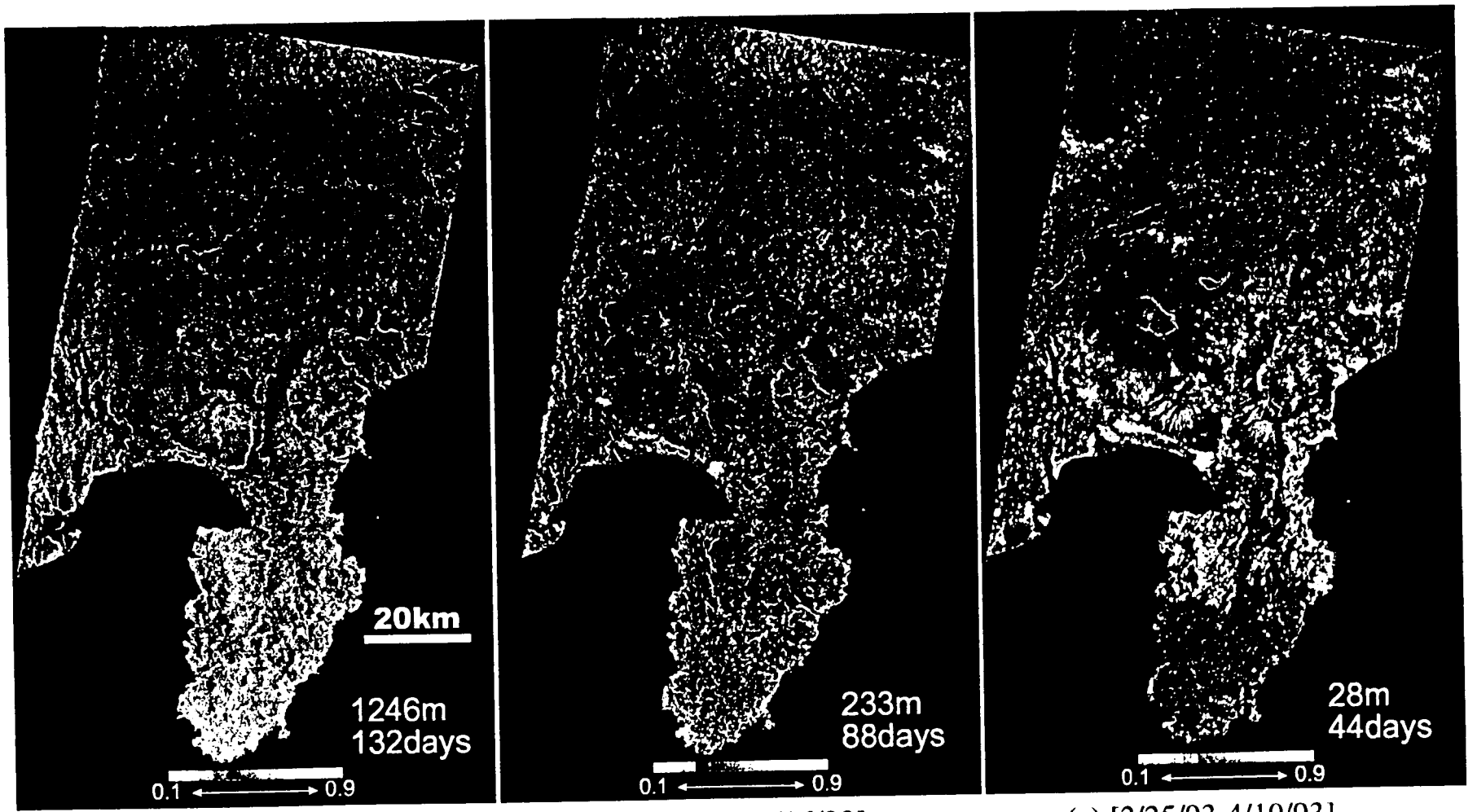

(a) [4/10/93-8/20/93] (b) [8/20/93-11/16/93] (c) [2/25/93-4/10/93]

Plate 3 Fujiwara et al., 1997

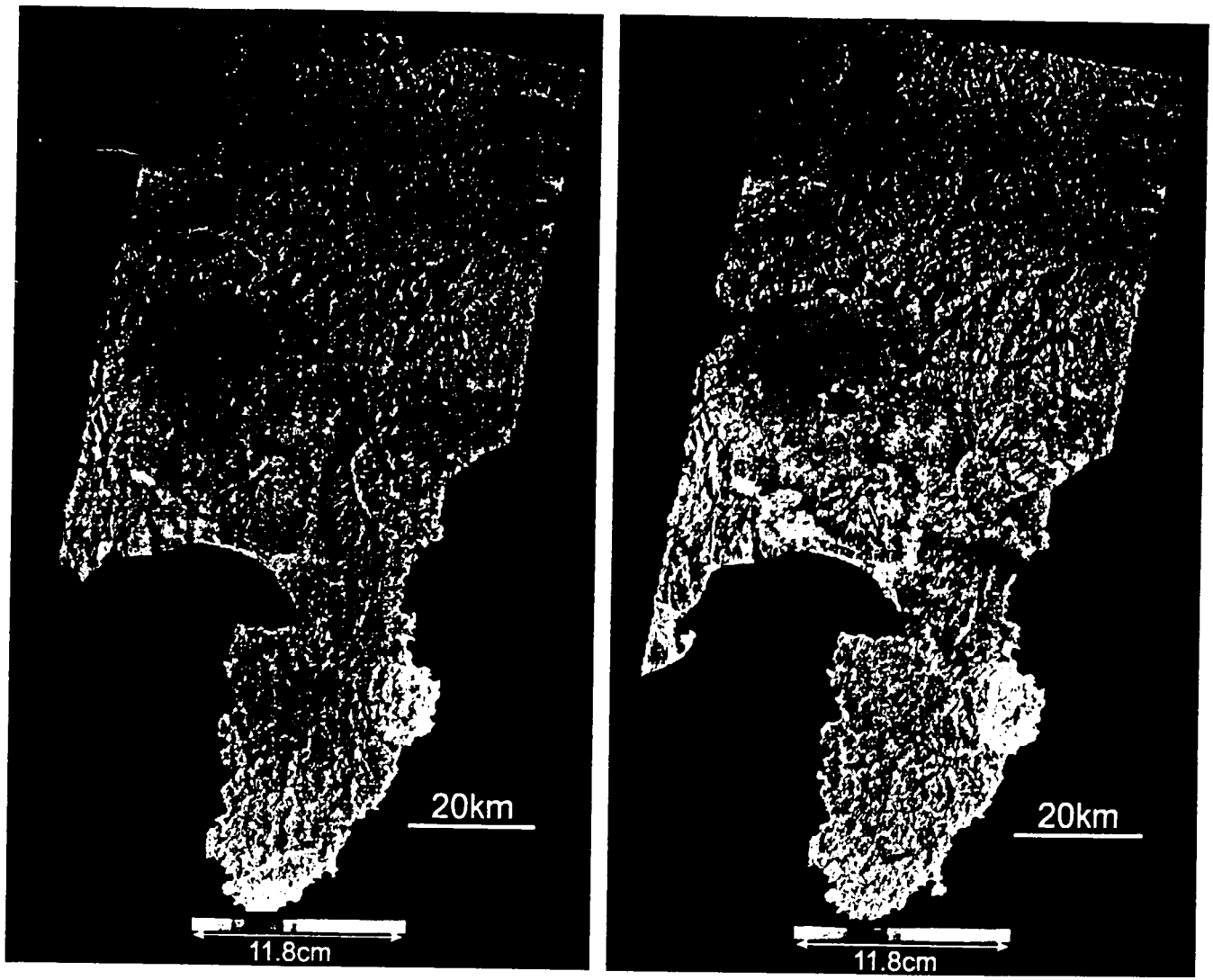

(a) (b)

Plate 4 Fujiwara et al., 1997